Nano Research

Open Access

Research Article

Enhanced energy storage density with improved self-healing property by biaxial orientation of 2D nanosheet composite polypropylene film

Zhiyuan Li[1], Xinyu Liu[1], Yuxin Cui[1], Yihan Zhou[1], Hongbo Liu[1], Zhicheng Zhang[2], Yao Zhou[1], Lu Cheng[1] ✉, and Wenfeng Liu[1] ✉

[1] *State Key Laboratory of Electrical Insulation and Power Equipment, School of Electrical Engineering, Xi'an Jiaotong University, Xi'an 710049, China*
[2] *National Innovation Platform (Center) for Industry-Education Integration of Energy Storage Technology, School of Chemistry, Xi'an Jiaotong University, Xi'an 710049, China*

Cite this article: *Nano Research*, **2025**, *18*, 94907447. https://doi.org/10.26599/NR.2025.94907447

ABSTRACT: Dielectric materials with enhanced energy storage performances are urgently demanded owing to the development of advanced capacitor equipment. However, low energy density and weak self-healing capabilities of current dielectric materials still limit the practical applications. Here, a biaxially oriented (polypropylene/two-dimensional (2D) Al_2O_3 nanosheets/grafted polypropylene) nanocomposite was proposed. The biaxial orientation enabled the directional arrangement of nanosheets in the polymer matrix. The oriented 2D nanosheets played a dominate role in the restriction of charge transportation and the tradeoff of energy consumption during breakdown and self-healing. Therefore, on one hand, the discharge energy density reached a considerable value of 9.64 J/cm³. On the other hand, the self-healing area of the metalized films was a 36% smaller than that of biaxially oriented polypropylene (BOPP) at the comparable self-healing energy, which was related to the long-term reliability of capacitor. The further experiments and simulations indicated that the oriented γ-A_2O_3 nanosheets (AONs) arrangement suppressed electric field distortion and hindered the charge transportation, which greatly enhanced the breakdown strength and ultimately improved the energy storage performance. This strategy presented a potential solution for improving the energy storage performance of capacitor films, which is suitable for current industrial production.

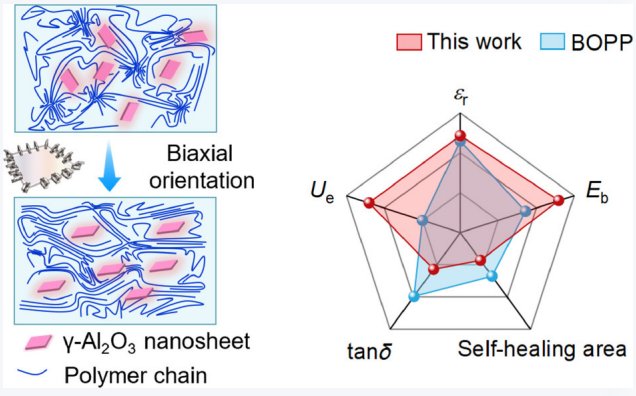

KEYWORDS: film capacitor, biaxially oriented polypropylene, capacitive energy storage, self-healing

1 Introduction

The metalized film capacitors are widely used in the advanced power equipment such as electric vehicles, high voltage direct current (DC) transmission, and electromagnetic weapons, due to the advantages of ultra-high applied electric field and low dielectric loss [1–4]. As the most advanced insulating material for metallized film capacitors on market, biaxially oriented polypropylene (BOPP) films exhibit the features of high breakdown strength, low-level tanδ, unique self-healing properties and large-scale processability, which ensure the high applied electric field and long-term reliability for capacitors [5–9]. Nevertheless, the energy storage density (U_e) of BOPP is around 3–4 J/cm³ at 600 kV/mm, which results in large size and weight of capacitors [10, 11]. For instance, the capacitor could occupy ~ 35 vol.% and ~ 23 wt.% of the inverter in electrical vehicles [12, 13]. Hence, it is imperative to increase the energy storage density of BOPP due to the demand for miniaturization and lightweight of the advanced metalized film capacitors.

In recent decades, extensive researches have been conducted to improve the energy storage density of dielectric materials. Among the numerous modification strategies [14–21], the method of

Received: February 11, 2025; **Revised:** March 10, 2025
Accepted: April 7, 2025

✉Address correspondence to Lu Cheng, chenglu@xjtu.edu.cn; Wenfeng Liu, liuwenfeng@xjtu.edu.cn

incorporation of nanofiller is considered as one of the most promising solutions [22–25]. For example, by adding nonpolar TiO_2 nanoparticles, the PP nanocomposite exhibited the discharged energy density of 4.19 J/cm³ [26]. Moreover, the energy storage density could be noticeably boosted by constructing oriented distribution of two-dimensional (2D) nanofillers, which has also been verified in other polymer materials, such as polyetherimide (PEI) and polyvinylidene fluoride (PVDF) [27–31]. While the 2D nanosheets could be introduced into PP matrix by blending and hot-pressing [32], it was difficult to make the 2D nanosheets form regular arrangement during biaxial orientation due to the incompatibility between the nanofillers and PP matrix [33]. The incompatibility would lead to the emergence of defects and a decreased breakdown strength for BOPP films [33–38]. Furthermore, a ternary composite strategy was proposed to optimize the compatibility between nanofillers and PP matrix. Nanoparticles with different dielectric properties were incorporated into the matrix of PP and grafted PP [39–41]. It proved to show that the ternary strategy significantly improved the molecular interaction between nanoparticles and polymer matrix, which resulted in the enhanced breakdown strength (BDS) and processibility for orientation [42]. Therefore, it is worthwhile to utilize the ternary strategy and biaxial orientation to construct the oriented arrangement of 2D nanosheets, which can exploit its advantages in improving energy storage density for BOPP films.

In the present study, we prepared a biaxially oriented PP-based composite film comprising 2D γ-A_2O_3 nanosheets (AONs) and grafted polypropylene (BO(PP/AA/AONs)). The obtained modified BOPP films exhibited simultaneously enhancement of energy storage density and self-healing property. On one hand, the effect of the directed stretching force constructed an oriented arrangement of AONs, thereby enhancing the breakdown strength and energy storage density. On the other hand, the grafting modified PP chains were introduced to optimize the compatibility between nanosheets and polymer matrix, which ensured the production of defect-free BOPP films. Moreover, more energy was consumed to destroy the ionic bond of AONs in the composite films when self-healing breakdown occurred, which in turn reduced the electrode loss of self-healing. This strategy demonstrated a considerable energy storage density of 9.64 J/cm³ with an over 30% smaller self-healing area compared with BOPP. The related experiments and simulations were conducted to reveal the mechanism of the enhanced energy storage performances. The synergistic improvement of energy storage density and self-healing property of ternary system showed the potential for practical applications for metalized film capacitors.

2 Results and discussion

2.1 The microstructure of the nanocomposites

The preparation of the composite film was illustrated in Fig. 1. The 2D AONs and the polypropylene grafted with acrylic acid (PP-g-AA) were synthesized by hydrothermal reaction and solution method [27, 41]. Subsequently, the composite films were obtained by the process of melt blending, hot-pressing, and biaxial

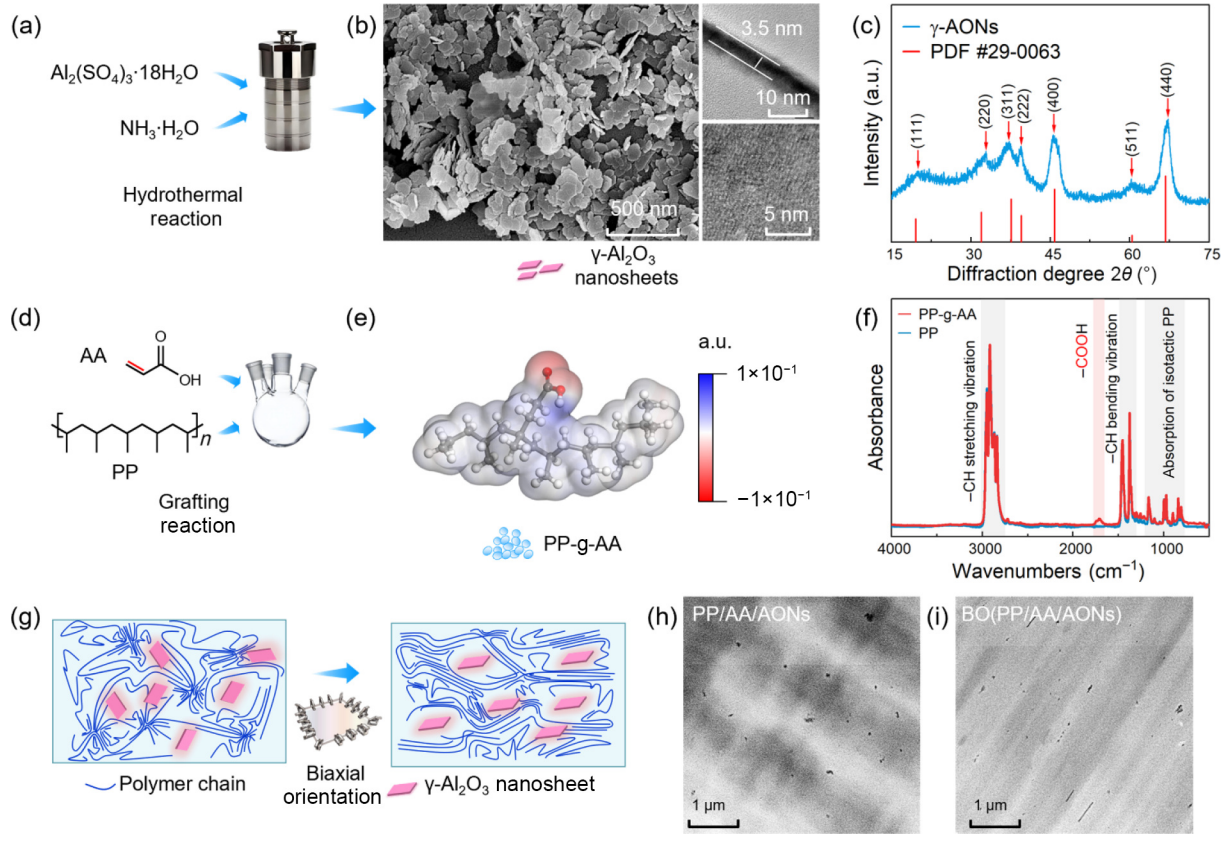

Figure 1 Schematic of preparation of BO(PP/AA/AONs) composite. (a) Preparation of γ-AONs by hydrothermal reaction, (b) SEM and TEM images of the obtained 2D nanofillers, and (c) XRD pattern of the obtained γ-AONs. (d) Preparation of PP-g-AA by solution method, (e) electrostatic potential distribution of PP-g-AA, and (f) FTIR spectra of the obtained PP-g-AA and pure PP. (g) Schematic of the difference between raw samples (PP/AA/AONs) and the biaxially oriented samples (BO(PP/AA/AONs)). (h) and (i) The cross-sectional images of the raw samples and biaxially oriented samples.

orientation. The biaxially oriented binary films consisted of PP and AONs with different doping contents of 0.5 wt.%, 1 wt.%, 3 wt.%, and 5 wt.%. The ternary composite (BO(PP/AA/AONs)) was composed of PP/PP-g-AA/AONs, where the content of AONs was 0.5 wt.%.

Firstly, the morphology and structure of the AONs were verified by scanning electron microscopy (SEM), transmission electron microscopy (TEM), and X-ray diffraction curves (XRD), as displayed in Figs. 1(b) and 1(c). The width of the AONs was around 50–350 nm, with a minimum thickness of 3.5 nm. The local high-resolution magnified image of TEM indicated the AONs possessed a relatively regular crystal structure. The further X-ray diffraction peaks of obtained AONs were located at crystal plane of (311), (400), and (440), which corresponded to the typical spinel lattice structure of γ-Al_2O_3 (JCPDS #29-0063) [43]. Besides, the PP-g-AA was conducted by the solution method and was verified by the Fourier transform infrared (FTIR) spectrum, as shown in Fig. 1(f). Compared with pure PP, the FTIR spectrum of PP-g-AA exhibited an extra peak at 1712 cm^{-1} which suggested the AA monomer was successfully grafted [44]. Besides, the polar AA groups exhibited the negative and positive electrostatic potential region, as shown in Fig. 1(e), which acted as a deep trap to attract charge carriers and was beneficial for the insulation performance of the composite [35, 41].

Moreover, the distribution and arrangement of the AONs in the matrix would be significantly changed by the biaxially oriented force. Hence, the cross-section images of the raw sample (PP/AA/AONs) and the biaxially oriented sample (BO(PP/AA/AONs)) were obtained by TEM to confirm the arrangement of AONs. Figure 1(h) indicated that the arrangement of AONs was random and disordered in the raw sample. On the contrary, in BO(PP/AA/AONs), the AONs presented a directional and parallel arrangement, as shown in Fig. 1(i). These results indicated that the force field during the biaxially oriented process made the AONs develop an oriented arrangement parallel to the plane of the films.

For BOPP, the aggregation structure and chain structure would undergo significant changes. The biaxial orientation would lead to the parallel arrangement of the molecular chains along the direction of the external force field, which caused the orientation of the polymer chains and segments. Therefore, the average orientation factor (f) and the orientation degree in the thickness direction (f_z) were obtained to analyze the orderliness of chains before and after biaxial orientation, based on the circular dichroism method [45–47]. As shown in Fig. 2(a), the orientation degree (both f and f_z) of BO(PP/AA/AONs) remarkably increased compared with PP/AA/AONs. The higher orientation degree implied a more regular arrangement and a higher orderliness of the molecular chains. The enhanced orderliness of chains structure would improve the activation energy of molecular chain segment motion and hinder the transportation of charge carriers, which improved breakdown strength [42].

In addition, the effect of biaxial orientation on the aggregated structure of PP was investigated by the differential scanning calorimetry (DSC) and the wide-angle X-ray diffraction (WAXD). As shown in Fig. 2(b), the heat flow curves of the first and second melting process were presented. The first melting process could reflect the influence of biaxial orientation on the thermodynamic properties, while the second melting process eliminated this influence and reflected the thermal properties of the raw condition. The melting temperature (T_m) of biaxially oriented samples increased compared with raw condition. The increased T_m indicated that the biaxially oriented samples exhibited larger lamella thickness, corresponding to a more stable thermodynamic property and a more regular molecular chain arrangement. Besides, the WAXD results presented that the biaxial orientation would evidently change the property of crystal region. On one hand, the diffraction intensity of the crystal face (110), (130), (111) and (041) decreased while the intensity of crystal face (040) increased. On the other hand, the crystallinity (X_c%) of the biaxially oriented samples increased compared with the raw samples. The coupling effect of temperature and force during the biaxial orientation led to the transformation of crystal form, recrystallization for amorphous, and the rearrangement of molecular chains. Furthermore, the transformation of crystal face and the increased X_c% indicated that the biaxial orientation led to a more regular aggregated structure, which further limited the charge transportation and improved the breakdown strength for BOPP.

2.2 Energy storage performance

For PP-based composite films, the maximum energy storage density (U_e) depended on the dielectric constant (ε_r) and the DC breakdown strength (BDS) [48]. Hereinto, the frequency-dependent dielectric constant (ε_r) and dielectric loss (tanδ) of composites were firstly studied, as shown in Fig. 3(a). The tanδ of all the samples maintained a low level around 1×10^{-3}. The enhanced interaction between the inorganic AONs and the PP-g-AA restricted the transportation of charge carriers and limited the conductivity. Hence, in the low-frequency region (0.1–1 Hz) where the conductivity loss dominated, the ternary samples exhibited a lower tanδ value (0.0019) than that of pure BOPP (0.0033). Likewise, the introduction of AONs and PP-g-AA played a dominant role in the increase of the dielectric constant. The dielectric constant of BO(PP/AA/AONs) and BO(PP/AONs) was 2.43 and 2.30, respectively, at 1 Hz, which were both higher than BOPP.

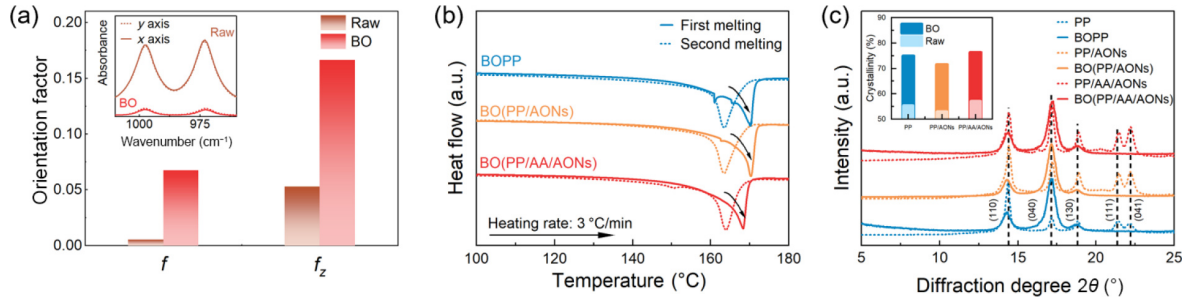

Figure 2 The structure change between the raw films and biaxially oriented samples. (a) The orientation degree of BO(PP/AA/AONs) and PP/AA/AONs obtained based on the circular dichroism method. (b) The DSC curves and (c) WAXD results and the crystallinity of the raw samples and biaxially oriented samples.

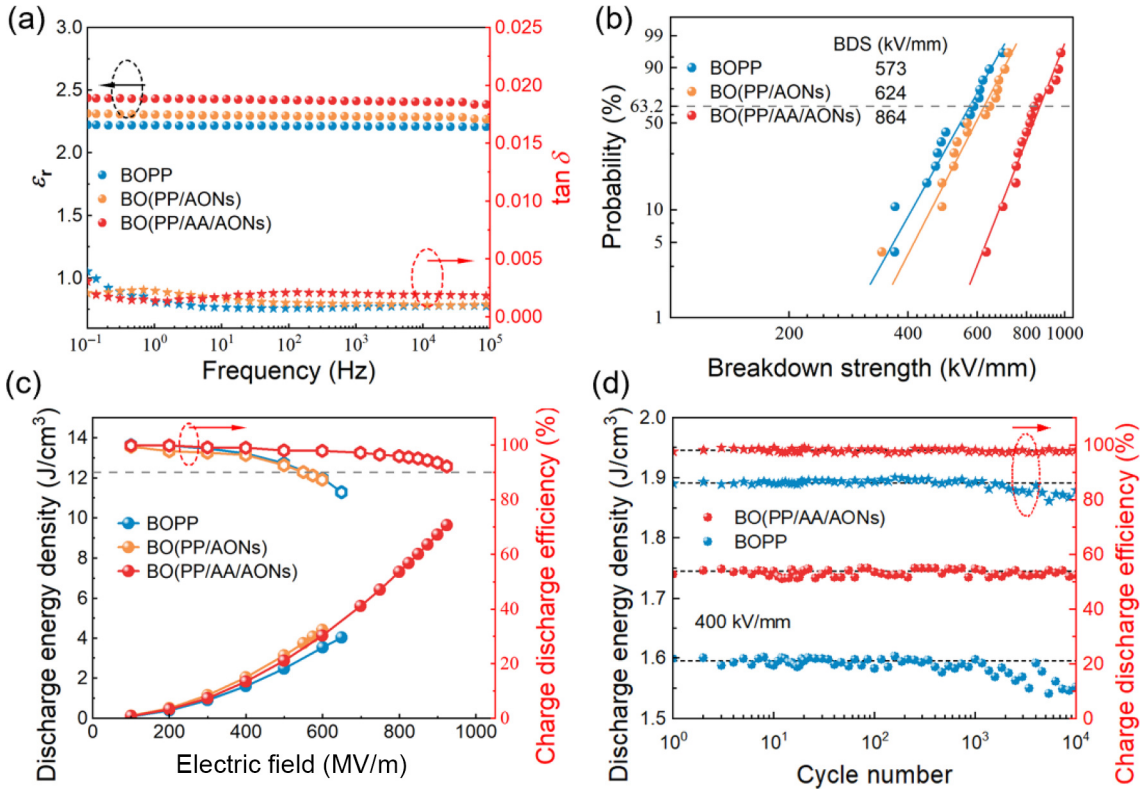

Figure 3 (a) Dielectric constant and loss response to frequency at room temperature. (b) Weibull distribution of breakdown strength. (c) Discharge energy density and energy storage efficiency of the composites at room temperature. (d) Cycling performance at 400 kV/mm and room temperature.

Subsequently, the DC breakdown experiment was conducted and the BDS was obtained by the 2-parameter Weibull distribution [49]. Figure 3(b) displayed that the ternary composite of BO(PP/AA/AONs) exhibited the superior BDS. The max BDS reached up to 864 kV/mm, which was 50% higher than the BOPP and 42% higher than the binary composite. On one hand, the binary composite was unfavorable for the production of defect-free films, which has been revealed in previous research [34, 36, 42]. The physical defects such as cavitation and void limited the blocking effect of nanosheets on breakdown development for the binary composite. On the other hand, the interaction between inorganic nanofillers and the PP-g-AA restricted the transportation of charge carriers [41, 50]. Therefore, the ternary composite exhibited the superior BDS and has a positive prospect for large-scale production.

Consistent with the dielectric property and breakdown strength, the U_e and efficiency (η) of the ternary nanosheet composite exhibited striking advantages. As displayed in Fig. 3(c), the maximum energy density of BOPP, BO(PP/AONs), and BO(PP/AA/AONs) were 4.0, 4.41, and 9.64 J/cm^3, respectively. The U_e of BO(PP/AA/AONs) was 140% higher than that of pure BOPP. More importantly, the charge–discharge efficiency of ternary composite was maintained above 90%. In addition, the charge-discharge cycling experiment was conducted to verify the cyclability of the composite at high electric field, as shown in Fig. 3(d). At room temperature and the electric field of 400 kV/mm, the BO(PP/AA/AONs) exhibited outstanding cycling endurance. Compared with BOPP, the ternary composites survived continuous 10^4 cycles without the indication of a decrease in U_e and η. The excellent cycling properties originated from the suppressed tanδ which limited the generation and accumulation of Joule heat during the long-term cycles. Compared with the reported performance of PP-based films, this work exhibited remarkable energy storage density and possessed dielectric loss comparable to pure BOPP films. These properties combined with the processibility of the biaxially oriented films enabled further applications on the polymer film capacitor.

2.3 Charge transportation characteristics

To further investigate the mechanism of the enhanced performance, the finite element simulation about the electric field distortion and breakdown path development was conducted. As shown in Figs. 4(a) and 4(b), the random distribution of AONs would cause significant partial field distortion around the nanosheets, which would make it easy for charge carries to transport along the electrical filed and thus lead to breakdown. On the contrary, the AONs with regular distribution parallel to plane of the films exhibited a uniform electric field distribution and restricted the charge transportation and breakdown development. Subsequently, based on the phase-filed model for the breakdown in solid dielectric [51, 52], a parameter s was introduced to characterize the status of breakdown path. Parameter s = 0 indicated the origin state, while s = 1 represented the damaged state. As shown in Figs. 4(c) and 4(d), the nanosheets AONs with regular and parallel arrangement would notably hinder the development of breakdown. However, the AONs with random arrangement failed to produce such a positive effect. Therefore, the ternary strategy and biaxial orientation fully utilized the advantage of constructing oriented nanosheets arrangement for improving BDS in PP matrix.

Moreover, the thermally stimulated depolarization current (TSDC) tests were carried out to reveal the correlation between charge transportation and charge trap energy levels based on the theoretical formula [53]. For PP-based composite, the peaks of

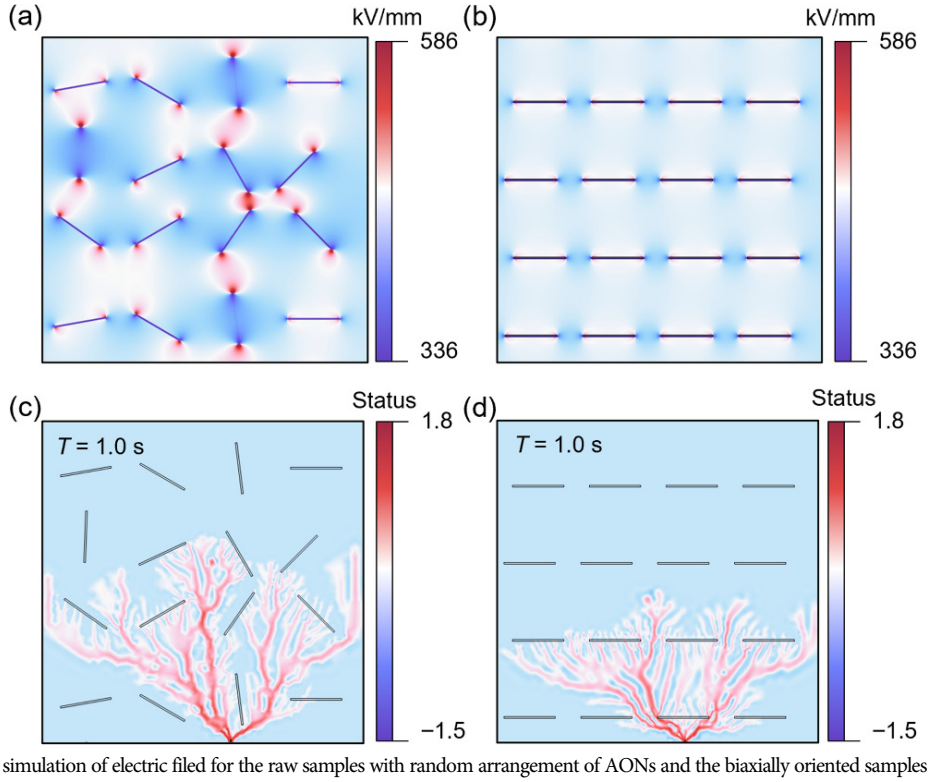

Figure 4 (a) and (b) The simulation of electric filed for the raw samples with random arrangement of AONs and the biaxially oriented samples with oriented and regular arrangement of AONs. (c) and (d) The simulation of breakdown path development for the raw sample and biaxially oriented sample.

leakage (80–140 °C, peak α) is determined by the charge transportation process which could be used to analyze the trap depth of charge carriers [54]. As pictured in Figs. 5(a)–5(c), for peak α, the biaxially oriented samples exhibited two deep trap energy levels (α_1 and α_2). The deepest trap energy level of pure BOPP was 1.60 eV, while that of BO(PP/AA/AONs) was 2.36 eV. For peak β (around the glass transition temperature of PP), the incorporation of grafted PP would introduce a large number of polar groups, which increased its depolarization leakage current density, as shown in Fig. 5(c).

Besides, the time-dependent DC leakage current at 90 °C and fixed electric field was measured and the DC conductivities of the samples were obtained. The samples with AONs exhibited a lower leakage current and a lower DC conductivity (γ) compared with BOPP, while the ternary composite BO(PP/AA/AONs) processed the lowest γ of 2.6×10^{-14} S/m. The decreased conductivity was attributed to the restricted the charge carries mobility, which shortened the hopping distance and hindered the energy accumulation of the electrons which in turn enhanced the BDS [55]. The inhibited charge transportation further limited the conductivity loss in the frequency range of 0.1 to 1 Hz, where the ternary composite exhibited the lower tanδ compared with BOPP.

Therefore, the enhancement mechanism of the energy storage performance of BO(PP/AA/AONs) was revealed. From the perspective of trap energy level, the introduction of oriented AONs and polar group of PP-g-AA significantly increased the deep trap energy level by about 0.76 eV compared with BOPP. The deeper trap energy level improved the ability to capture charge carriers and inhibited the trapped carries from detrapping, which impeded the directional transportation of carries and formed a shorter hopping distance and lower DC conductivity [56]. On the other hand, the oriented AONs arrangement was successfully constructed in the ternary composite, since the incompatibility between inorganic nanosheets and PP matrix was settled by the interaction between grafted polymer chains and nanofillers. The regular distribution fully exploited the blocking effect of the large aspect ratio nanosheets AONs, suppressed the electric field distortion and prevented the development of breakdown path. Hence, the biaxially oriented ternary composite exhibited the strikingly improved BDS and energy storage density.

2.4 Self-healing property

In parallel to the energy storage performance, the self-healing property of the metalized film is one of the concerns for polymer film capacitors [57, 58]. The self-healing process (SH) of the metalized films is based on the fact that the metalized film capacitors can restore the insulation performance after the electric breakdown occurs around the defect of the dielectric films [59]. When the breakdown occurs, the huge current would be generated and the adjoining Al/Zn-coated electrodes will be evaporated [60]. Thus, the defect becomes isolated and the insulation performance of the capacitor is restored. Therefore, the obtained thin films underwent the process of metal electrode coating and the experiments of SH property were conducted, as shown in Fig. 6.

First of all, the typical SH voltage–current waveforms were successfully monitored for BOPP and BO(PP/AA/AONs). Figure 6(a) showed that a large current was generated and quickly recovered to zero. However, the self-healing breakdown unit was unable to restore enough charge to recover the initial voltage value within the time range of 4 μs. The SH voltage took hundreds of microseconds to recover to its its initial value, depending on the time constant of self-healing circuit [61]. Therefore, the SH voltage firstly dropped and then slowly recovered. The energy of SH (W_{sh}) could be obtained by calculating the integral of the product of SH

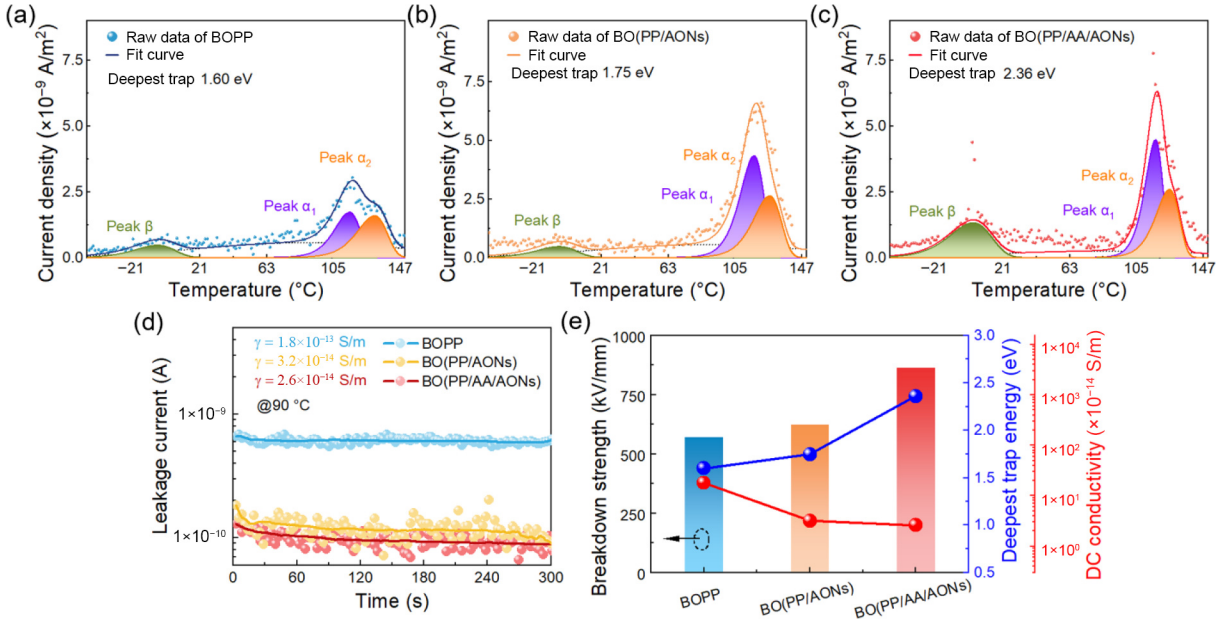

Figure 5 TSDC of (a) the biaxially oriented polypropylene, (b) the biaxially oriented PP/AONs, and (c) the biaxially oriented PP/AA/AONs. (d) Time-dependent DC leakage current of BOPP, BO(PP/AONs), and BO(PP/AA/AONs). (e) The relationship between the breakdown strength, deepest trap energy and DC conductivity.

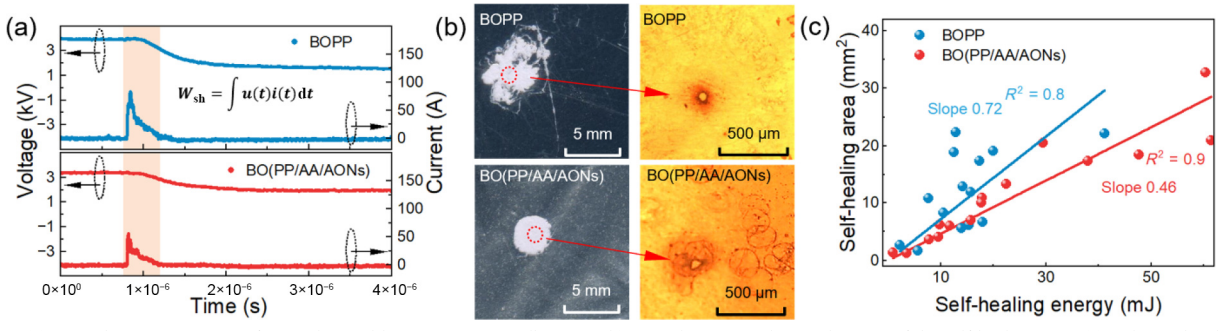

Figure 6 (a) SH voltage–current waveforms obtained by MSO4300 Oscilloscope. (b) Digital image and optical image of the self-healing area. (c) Relationship between self-healing area and self-healing energy.

voltage and SH current before the SH current depletion [62, 63]. The rectangular method in numerical integration was introduced to simplify the calculation. Then, the morphology and electrode clearness of the SH areas were observed by digital camera and optical microscope, as pictured in Fig. 6(b). Both the BOPP and BO(PP/AA/AONs) displayed the evident electrode clearness area and possessed the puncture hole which originated from the SH process of metalized films.

Moreover, based on the proportional relationship between the SH areas and energy [63], it was indicated that the SH areas of BO(PP/AA/AONs) exhibited smaller sizes compared with BOPP under the comparable value of W_{sh}, as shown in Fig. 6(c). The fitted slope of BO(PP/AA/AONs) results was 0.46, which was 36% smaller than that of BOPP. The results suggested that the electrode degradation of BO(PP/AA/AONs) was slighter than that of BOPP when the SH process occurred. This was because the W_{sh} included two parts: the energy used for electrode clearness and the energy consumed by damaging the films. For the ternary composite, the energy consumed by damaging the films increased compared with BOPP, since more energy was required to break ionic bond of AONs (15,900 J/mol, Al_2O_3) [64]. Thus, at the comparable value of W_{sh}, less energy was used for electrode clearness and the ternary sample exhibited a smaller SH area. The SH ability ensured the isolation of weak points for the biaxially oriented films and enhanced the stability for the capacitor. The less SH area of ternary system would cause a slighter capacitance loss for capacitor elements, which could improve the lifetime during the long-term operation [6].

3 Conclusion

In summary, the biaxially oriented PP-based thin film with giant energy storage density and excellent self-healing property was prepared. The obtained films exhibited an energy density of 9.64 J/cm^3 and a reduced self-healing area. Besides, the dielectric loss and cycling endurance of BO(PP/AA/AONs) composite films was comparable to those of pure BOPP films. The introduction of oriented AONs played a dominant role in the enhancement of energy storage density and self-healing property, which was investigated by simulations and experiments. These advantages indicated the modification of BOPP via grafting and oriented nanosheet compositing was a promising method for the large-scale production and long-term reliable application of capacitor films. For the further exploitation, the method for the scalable production of the grafted PP and parameter matching between modified resins and different biaxially oriented equipment must be taken into consideration.

Electronic Supplementary Material: Supplementary material (additional details including the preparation of samples, the method of characterization and simulation, SEM images, FTIR spectra, and the results of electrical experiments) is available in the online version of this article at https://doi.org/10.26599/NR.2025.94907447.

Data availability

All data needed to support the conclusions in the paper are presented in the manuscript and the Electronic Supplementary Material. Additional data related to this paper may be requested from the corresponding author upon request.

Acknowledgements

We thank Mr. Zhang Zhenguo, Ms. Duan Yerong, and Ms. Tan Fuchun at Instrument Analysis Center and School of Electrical Engineering of Xi'an Jiaotong University for their assistance. We appreciate computing support from Mr. Yang Fan and the Xi'an Jiaotong University campus level public high-performance computing service platform. Project supported by the National Natural Science Foundation of China (No. U24A20151)

Declaration of competing interest

All the contributing authors report no conflict of interests in this work.

Author contribution statement

Z. Y. L.: Conceptualization, methodology, investigation, formal analysis, writing – original draft, visualization. X. Y. L.: Methodology, investigation. Y. X. C.: Methodology, investigation. Y. H. Z.: Methodology. H. B. L.: Conceptualization. Z. C. Z.: Resources. Y. Z.: Writing – conceptualization and review & editing. L. C.: Conceptualization, data curation, formal analysis, project administration, funding acquisition, writing – review & editing, visualization. W. F. L.: Funding acquisition, conceptualization, data curation, formal analysis, writing – review & editing, resources.

Use of AI statement

None.

References

[1] Wang, J. Q.; Guo, H. X.; Zeng, S. X.; Du, J. Q.; Zhang, Q.; Wang, K. Thin, largescale processed, high-temperature resistant capacitor films based on polypropylene/cycloolefin copolymer blend. *Chem. Eng. J.* **2024**, *492*, 152237.

[2] Li, X. H.; Liu, B.; Wang, J.; Li, S. X.; Zhen, X.; Zhi, J. P.; Zou, J. J.; Li, B.; Shen, Z. H.; Zhang, X. et al. High-temperature capacitive energy storage in polymer nanocomposites through nanoconfinement. *Nat. Commun.* **2024**, *15*, 6655.

[3] Yang, M. C.; Wang, S. J.; Fu, J.; Zhu, Y. J.; Liang, J. J.; Cheng, S.; Hu, S. X.; Hu, J.; He, J. L.; Li, Q. Quantum size effect to induce colossal high-temperature energy storage density and efficiency in polymer/inorganic cluster composites. *Adv. Mater.* **2023**, *35*, 2301936.

[4] Zeng, T.; Li, Q.; Liu, D. D.; Fu, J.; Zhong, L. P.; He, J. L.; Li, Q.; Yuan, C. Improved capacitive energy storage performance in hybrid films with ultralow aminated molybdenum trioxide integration for high-temperature applications. *Mater. Horiz.* **2024**, *11*, 1539–1547.

[5] Wu, Z. Y.; Liu, S. S.; Tong, T.; Zhong, S. L.; Wang, J. T.; Qi, H. B.; Dang, Z. M.; Wang, W. Theoretical and experimental studies on the self-healing properties of metallised capacitor films under multiple stresses. *High Volt.* **2024**, *9*, 1347–1356.

[6] Li, Z. Y.; Zhou, Y. H.; Wang, X. G.; Liu, H. B.; Cheng, L.; Liu, W. F.; Li, S. T.; Guo, J.; Xu, Y. Failure mechanism of metallized film capacitors under DC field superimposed ac harmonic: From equipment to material. *High Volt.* **2024**, *9*, 1081–1089.

[7] Qin, H. M.; Liu, M.; Li, Z. W.; Fu, Y. H.; Song, J. H.; Xie, J.; Xiong, C. X.; Wang, S. Cycloolefin copolymer dielectrics for high temperature energy storage. *J. Energy Storage* **2022**, *55*, 105756.

[8] Zhu, J. F.; Tong, H.; Cao, S. M.; Luo, J. P.; Liu, X. P.; Xu, J.; Oleksandr, M.; Peng, W. F. Self-healing behaviors of metallized high-temperature dielectric films for capacitor applications. *Microelectron. Reliab.* **2023**, *144*, 114972.

[9] Wang, Y. W.; Bao, Z. W.; Ding, S.; Jia, J. H.; Dai, Z. Z.; Li, Y. X.; Shen, S. C.; Chu, S. C.; Yin, Y. W.; Li, X. G. γ-ray irradiation significantly enhances capacitive energy storage performance of polymer dielectric films. *Adv. Mater.* **2024**, *36*, 2308597.

[10] Li, X. Y.; Xie, Y. C.; Xiong, J.; Zhu, B. F.; Zhang, X.; Duan, X. H.; Dong, B.; Zhang, Z. C. Superior high-temperature capacitive performance of polyaryl ether ketone copolymer composites enabled by interfacial engineered charge traps. *Mater. Horiz.* **2023**, *10*, 5881–5891.

[11] Ma, G. Q.; Yang, T. B.; Li, D. L.; Lv, J. C.; Jia, D. Z.; Li, Y.; Xu, L.; Huang, H. D.; Zhong, G. J.; Li, Z. M. Toward excellent energy storage performance via well-aligned and isolated interfaces in multicomponent polypropylene-based all-organic polymer dielectric films. *ACS Appl. Mater. Interfaces* **2023**, *15*, 23701–23710.

[12] Chen, Q.; Shen, Y.; Zhang, S. H.; Zhang, Q. M. Polymer-based dielectrics with high energy storage density. *Annu. Rev. Mater. Res.* **2015**, *45*, 433–458.

[13] Cui, Y.; Feng, Y.; Zhang, T. D.; Zhang, C. H.; Chi, Q. G.; Zhang, Y. Q.; Wang, X.; Chen, Q. G.; Lei, Q. Q. Excellent energy storage performance of ferroconcrete-like all-organic linear/ferroelectric polymer films utilizing interface engineering. *ACS Appl. Mater. Interfaces* **2020**, *12*, 56424–56434.

[14] Huang, B. D.; Yu, J. C.; Dong, J.; Zhou, Y.; Zhai, L.; Dou, L. G.; Wu, C.; Liang, X. D.; Zhang, C.; Ostrikov, K. et al. Improving charge storage of biaxially-oriented polypropylene under extreme electric fields by excimer UV irradiation. *Adv. Mater.* **2024**, *36*, 2311713.

[15] Li, Z. C.; Zhang, Y.; Pan, Z. B.; Fan, X.; Li, P.; Huang, H. M.; Wang, W. L.; Chen, W. D.; Liu, J. J.; Li, W. P. Optimizing the gradient of electric field distribution and inhibiting charge injection in multilayer dielectric films for high capacitive performance. *J. Mater. Chem. A* **2024**, *12*, 3616–3622.

[16] Li, J. L.; Wang, S. J.; Zhu, Y. J.; Luo, Z.; Zhang, Y. R.; Shao, Q.; Quan, H.; Wang, M. T.; Hu, S. X.; Yang, M. C. et al. Biaxially oriented films of grafted-polypropylene with giant energy density and high efficiency at 125 °C. *J. Mater. Chem. A* **2023**, *11*, 10659–10668.

[17] Yu, S. Q.; Zhou, J. L.; Xu, A.; Lao, J. J.; Luo, H.; Chen, S. The scalable and high performance polyimide dielectrics containing alicyclic structures for high-temperature capacitive energy storage. *Chem. Eng. J.* **2023**, *469*, 143803.

[18] Zhou, Y.; Chen, Y. H.; Cui, Y. X.; Li, Y. Z.; Li, Z. Y.; Zhou, C. W.; Cheng, L.; Liu, W. F. Scalable polyolefin-based all-organic dielectrics with superior high-temperature capacitive energy storage performance. *Energy Storage Mater.* **2024**, *72*, 103715.

[19] Li, Y. S.; Cheng, S.; Wang, S. J.; Yuan, C.; Luo, Z.; Zhu, Y. J.; Hu, J.; He, J. L.; Li, Q. Multilayered ferroelectric polymer composites with high energy density at elevated temperature. *Compos. Sci. Technol.* **2021**, *202*, 108594.

[20] Li, W. X.; Wang, Q. W.; Zhang, G. X.; He, Y. J.; Qin, B.; Zhang, X.; Liu, Z. X.; Gong, H. H.; Zhang, Z. C. Ultrahigh energy density achieved at high efficiency in dielectric capacitors by regulating α-phase crystallization in polypropylene films with fluorinated groups. *Adv. Funct. Mater.* **2024**, *34*, 2410959.

[21] Sima, W. X.; Mai, Y. X.; Sun, P. T.; Yang, M.; Yuan, T.; Chen, B. H.; Yang, Y. H. Achieving exceptional high-temperature capacitance energy storage in polyimide through aromatic structure-based electron induced effects. *Energy Storage Mater.* **2025**, *74*, 103974.

[22] Sun, H.; Zhang, T. D.; Yin, C.; Sun, H. Z.; Zhang, C. H.; Zhang, Y.; Zhang, Y. Q.; Tang, C.; Chi, Q. G. Significantly enhanced high-temperature energy storage performance for polymer composite films with gradient distribution of organic fillers. *Chem. Eng. J.* **2024**, *497*, 154546.

[23] Zheng, M. S.; Zheng, Y. T.; Zha, J. W.; Yang, Y.; Han, P.; Wen, Y. Q.; Dang, Z. M. Improved dielectric, tensile and energy storage properties of surface rubberized $BaTiO_3$/polypropylene nanocomposites. *Nano Energy* **2018**, *48*, 144–151.

[24] Xie, H. R.; Luo, H.; Pei, Z. T.; Chen, S.; Zhang, D. Improved discharge energy density and efficiency of polypropylene-based dielectric nanocomposites utilizing $BaTiO_3$@TiO_2 nanoparticles. *Mater. Today Energy* **2022**, *30*, 101160.

[25] Liu, B.; Yang, M. H.; Zhou, W. Y.; Cai, H. W.; Zhong, S. L.; Zheng, M. S.; Dang, Z. M. High energy density and discharge efficiency polypropylene nanocomposites for potential high-power capacitor. *Energy Storage Mater.* **2020**, *27*, 443–452.

[26] Li, S. H.; Pan, J. H.; Luo, B. C.; Wang, C.; Cai, Z. M.; Zhu, C. Q.; Zhang, B. J.; Kang, X. Q.; Zhou, D. P.; Liu, J. L. et al. Nonpolar sub-10 nm TiO_2 nanocrystal for high energy density polypropylene nanocomposites. *Nano Energy* **2024**, *121*, 109237.

[27] Ai, D.; Han, Y. T.; Xie, Z. L.; Pang, X.; Chang, Y.; Li, H.; Wu, C. L.; Cheng, Y. H.; Wu, G. L. High temperature polyimide nanocomposites containing two-dimensional nanofillers for improved thermal stability and capacitive energy storage performance. *Nano Res.* **2024**, *17*, 7746–7755.

[28] Yang, X.; Xuan, L. X.; Men, W. W.; Wu, X.; Lan, D.; Shi, Y. P.; Jia, H. X.; Duan, Y. P. Carbonyl iron/glass fiber cloth composites: Achieving multi-spectrum stealth in a wide temperature range. *Chem. Eng. J.* **2024**, *491*, 151862.

[29] Xie, B.; Zhang, H. B.; Zhang, Q.; Zang, J. D.; Yang, C.; Wang, Q. P.; Li, M. Y.; Jiang, S. L. Enhanced energy density of polymer nanocomposites at a low electric field through aligned $BaTiO_3$ nanowires. *J. Mater. Chem. A* **2017**, *5*, 6070–6078.

[30] Li, H.; Yang, T. N.; Zhou, Y.; Ai, D.; Yao, B.; Liu, Y.; Li, L.; Chen, L. Q.; Wang, Q. Enabling high-energy-density high-efficiency ferroelectric polymer nanocomposites with rationally designed nanofillers. *Adv. Funct. Mater.* **2021**, *31*, 2006739.

[31] Liu, X. X.; Chen, D. Y.; Li, J. L.; Zhong, S. L.; Feng, Y.; Yue, D.; Sheng, D. W.; Chen, H. N.; Hao, X. D.; Dang, Z. M. Atomic-level matching metal-ion organic hybrid interface to enhance energy storage of polymer-based composite dielectrics. *Adv. Mater.* **2024**, *36*, 2402239.

[32] Wang, C. Y.; Xing, Z. L.; Yan, S. Y.; Shi, L. R.; Hao, C. C.; Lei, Q. Q. Dielectric film with high energy density based on polypropylene/maleic anhydride-grafted polypropylene/boron nitride nanosheet ternary system. *Mater. Res. Bull.* **2022**, *155*, 111978.

[33] Xie, Z. L.; Zhu, J. A.; Dou, Z. L.; Zhang, Y. Z.; Wang, K.; Wu, K.; Fu, Q. Liquid metal interface mechanochemistry disentangles energy density and biaxial stretchability tradeoff in composite capacitor film. *Nat. Commun.* **2024**, *15*, 7817.

[34] Rytöluoto, I.; Niittymäki, M.; Seri, P.; Naderiallaf, H.; Lahti, K.; Saarimäki, E.; Flyktman, T.; Paajanen, M. Biaxially oriented silica-polypropylene nanocomposites for HVDC film capacitors: Morphology-dielectric property relationships, and critical evaluation of the current progress and limitations. *J. Mater. Chem. A* **2022**, *10*, 3025–3043.

[35] Meng, Z. T.; Zhang, T. D.; Zhang, C. H.; Shang, Y. A.; Lei, Q. Q.; Chi, Q. G. Advances in polymer dielectrics with high energy storage performance by designing electric charge trap structures. *Adv. Mater.* **2024**, *36*, 2310272.

[36] Rytöluoto, I.; Gitsas, A.; Pasanen, S.; Lahti, K. Effect of film structure and morphology on the dielectric breakdown characteristics of cast and biaxially oriented polypropylene films. *Eur. Polym. J.* **2017**, *95*, 606–624.

[37] Zhang, T. D.; Sun, H.; Yin, C.; Jung, Y. H.; Min, S.; Zhang, Y.; Zhang, C. H.; Chen, Q. G.; Lee, K. J.; Chi, Q. G. Recent progress in polymer dielectric energy storage: From film fabrication and modification to capacitor performance and application. *Prog. Mater. Sci.* **2023**, *140*, 101207.

[38] Du, B. X.; Cui, B. Effects of thermal conductivity on dielectric breakdown of micro, nano sized BN filled polypropylene composites. *IEEE Trans. Dielectr. Electr. Insul.* **2016**, *23*, 2116–2125.

[39] Cheng, L.; Liu, W. F.; Liu, H. B.; Li, S. T. Evolution of dielectric relaxation under elevated electric field of polypropylene-based films. *J. Phys. D: Appl. Phys.* **2020**, *53*, 445502.

[40] Cheng, L.; Liu, W. F.; Zhang, Z. Q.; Zhou, Y. C.; Li, S. T. Enhanced breakdown strength and restrained dielectric loss of polypropylene/maleic anhydride grafted polypropylene/core–shell ZrO_2@SiO_2 nanocomposites. *Polym. Compos.* **2022**, *43*, 2175–2183.

[41] Liu, W. F.; Liu, H. B.; Cheng, L.; Li, S. T. Enhanced energy storage performance in polypropylene-acrylic acid grafted polypropylene-ZrO_2 ternary nanocomposites. *J. Phys. D: Appl. Phys.* **2023**, *56*, 244001.

[42] Liu, W. F.; Li, Z. Y.; Liu, H. B.; Zhou, Y. H.; Zeng, J. K.; Zhao, Y.; Cheng, L.; Zhou, Y.; Li, S. T. Bi-axially oriented ternary polypropylene composite film with enhanced energy storage property at elevated temperature. *J. Mater. Chem. A* **2024**, *12*, 28531–28540.

[43] Parida, K. M.; Pradhan, A. C.; Das, J.; Sahu, N. Synthesis and characterization of nano-sized porous gamma-alumina by control precipitation method. *Mater. Chem. Phys.* **2009**, *113*, 244–248.

[44] Saffar, A.; Carreau, P. J.; Ajji, A.; Kamal, M. R. Development of polypropylene microporous hydrophilic membranes by blending with PP-g-MA and PP-g-AA. *J. Membr. Sci.* **2014**, *462*, 50–61.

[45] Fereydoon, M.; Tabatabaei, S. H.; Ajji, A. X-ray and trichroic infrared orientation analyses of uniaxially stretched PA6 and MXD6 nanoclay composite films. *Macromolecules* **2014**, *47*, 2384–2395.

[46] Garton, A.; Carlsson, D. J.; Wiles, D. M. Molecular orientation measurements in polymers by infrared spectral subtraction. *Appl. Spectrosc.* **1981**, *35*, 432–435.

[47] Shen, D. Y.; Molis, S. E.; Hsu, S. L. Vibrational spectroscopic characterization of rigid rod polymers: IV Crystalline modifications of poly(p-phenylene terephthalamide). *Polym. Eng. Sci.* **1983**, *23*, 543–547.

[48] Wang, S. J.; Luo, Z.; Liang, J. J.; Hu, J.; Jiang, N. S.; He, J. L.; Li, Q. Polymer nanocomposite dielectrics: Understanding the matrix/particle interface. *ACS Nano* **2022**, *16*, 13612–13656.

[49] Zhao, Y.; Liu, W. F.; Ran, D. S.; Jin, Y. H.; Li, Z. Y.; Zhong, C. Z.; Kong, F. Y.; Li, S. T. Lead-free (Ba,Sr)TiO_3-based ceramics with superior tunable properties by the semi-solution method. *J. Adv. Ceram.* **2024**, *13*, 746–756.

[50] Cheng, L.; Liu, W. F.; Liu, C. M.; Liu, X. W.; Li, S. T. Enhanced energy storage properties of polypropylene/maleic anhydride - grafted polypropylene/nano-ZrO_2 ternary system. *J. Appl. Polym. Sci.* **2019**, *136*, 48211.

[51] Chaitanya Pitike, K.; Hong, W. Phase-field model for dielectric breakdown in solids. *J. Appl. Phys.* **2014**, *115*, 044101.

[52] Deng, T.; Hu, T. F.; Liu, Z.; Yao, C. H.; Dai, K.; Cao, F.; Hu, Z. G.; Wang, G. S. Ultrahigh energy storage performance in BNT-based binary ceramic via relaxor design and grain engineering. *Energy Storage Mater.* **2024**, *71*, 103659.

[53] Cheng, L.; Liu, W. F.; Liu, X. W.; Liu, C. M.; Li, S. T.; Xing, Z. L.

Online degradation of biaxial-orientated polypropylene film from HVDC filter capacitors. *IEEE Trans. Dielectr. Electr. Insul.* **2019**, *26*, 26–33.

[54] Li, S. T.; Xie, D. R.; Qu, G. H.; Yang, L. Q.; Min, D. M.; Cheng, Y. H. Tailoring interfacial compatibility and electrical breakdown properties in polypropylene based composites by surface functionalized POSS. *Appl. Surf. Sci.* **2019**, *478*, 451–458.

[55] Chen, K.; Du, B. X.; Liu, H. L.; Xiao, M. Improved dielectric and energy storage performance of BOPP film by decreasing ambient temperature. *IEEE Trans. Dielectr. Electr. Insul.* **2025**, *32*, 1056–1063.

[56] Zhao, Z. H.; Feng, Y.; Yang, L. Q.; Zhang, S.; Liu, X.; Zhang, Y.; Li, M. R.; Li, S. T. Optimizing the conjugated structure of aromatic polyurea for high-temperature capacitive energy storage. *Appl. Phys. Lett.* **2023**, *123*, 232901.

[57] Tortai, J. H.; Bonifaci, N.; Denat, A.; Lesaint, O. Self-healing of aluminium metallized polypropylene films: A spectroscopic investigation. In *Proceedings of the 2002 IEEE 14th International Conference on Dielectric Liquids*, Graz, Austria, 2002, pp 190–193.

[58] Belko, V. O.; Emelyanov, O. A. Self-healing processes of metallized film capacitors in overload modes—Part II: Theoretical and computer modeling. *IEEE Trans. Plasma Sci.* **2021**, *49*, 1898–1905.

[59] Kammermaier, J.; Rittmayer, G.; Birkle, S. Modeling of plasma-induced self-healing in organic dielectrics. *J. Appl. Phys.* **1989**, *66*, 1594–1609.

[60] Peng, B.; Lin, F. H.; Li, H.; Chen, Y. H.; Zhang, M.; Lv, F. Calculation and measurement of metalized film capacitor's inner pressure and its influence on self-healing characteristics. *IEEE Trans. Dielectr. Electr. Insul.* **2010**, *17*, 1612–1618.

[61] He, Y. S.; Wang, F. P.; Du, G. Q.; Pan, L.; Li, J.; Yang, H. M.; Zhang, X.; Zhang, Z. C.; Wang, K. Z. Unveiling first self-healing in metallised film capacitor: A macro-micro analysis. *High Volt.*, in press, DOI: 10.1049/hve2.70005.

[62] Rytoluoto, I.; Lahti, K. New approach to evaluate area-dependent breakdown characteristics of dielectric polymer films. *IEEE Trans. Dielectr. Electr. Insul.* **2013**, *20*, 937–946.

[63] Belko, V. O.; Emelyanov, O. A.; Ivanov, I. O.; Plotnikov, A. P. Self-healing processes of metallized film capacitors in overload modes—Part 1: Experimental observations. *IEEE Trans. Plasma Sci.* **2021**, *49*, 1580–1587.

[64] Hornyak, G. L.; Dutta, J.; Tibbals, H. F.; Rao, A. Chemical interactions at the nanoscale. In *Introduction to Nanoscience*. Hornyak, G. L.; Dutta, J.; Tibbals, H. F.; Rao, A., Eds.; CRC Press: Boca Raton, 2008.

This is an open access article under the terms of the Creative Commons Attribution 4.0 International License (CC BY 4.0, https://creativecommons.org/licenses/by/4.0/).

© The Author(s) 2025. Published by Tsinghua University Press.